Modeling cluster formation driven variations in critical electric field of He and Xe near critical point based on electron scattering cross sections

Cite as: Phys. Fluids **32**, 127106 (2020); https://doi.org/10.1063/5.0028601
Submitted: 05 September 2020 . Accepted: 25 November 2020 . Published Online: 08 December 2020

Farhina Haque, Jia Wei (魏嘉), Alfonso Cruz, Lukas Graber, and Chanyeop Park (박 찬 엽)

Physics of Fluids ARTICLE scitation.org/journal/phf

Modeling cluster formation driven variations in critical electric field of He and Xe near critical point based on electron scattering cross sections

Cite as: Phys. Fluids 32, 127106 (2020); doi: 10.1063/5.0028601
Submitted: 5 September 2020 • Accepted: 25 November 2020 •
Published Online: 8 December 2020

Farhina Haque,[1] Jia Wei (魏嘉),[2] Alfonso Cruz,[2] Lukas Graber,[2] and Chanyeop Park (박찬엽)[1,a)]

AFFILIATIONS

[1] Department of Electrical and Computer Engineering, Mississippi State University, Mississippi State, Mississippi 39762, USA
[2] School of Electrical and Computer Engineering, Georgia Institute of Technology, Atlanta, Georgia 30313, USA

[a)] Author to whom correspondence should be addressed: chanyeop.park@ece.msstate.edu

ABSTRACT

The dielectric breakdown strength of supercritical He and supercritical Xe shows a steep decline near the critical point due to density fluctuation caused by cluster formation. Conventional gas discharge theories are limited in explaining the drastic dielectric strength variation of He and Xe near the critical point. In this study, a dielectric strength modeling approach that is based on the derived cross section data of clusters is utilized to estimate the dielectric strength decline of He and Xe near the critical point. The electron scattering cross section data of He and Xe clusters are derived from those of gaseous He and Xe. Based on the derived electron scattering cross section data, critical electric fields of various He and Xe clusters are modeled as a function of pressure by solving the Boltzmann equation. The proposed modeling approach shows close agreement with the experimentally measured breakdown electrical fields reported in the literature.

I. INTRODUCTION

High temperature superconducting (HTS) technology provides promising solutions to emerging aerospace and naval power applications that require light weight, high efficiency, and high power density. Conventionally, cryogenic conditions required by HTS applications have been achieved by using liquid nitrogen (LN_2) owing to its effective heat transfer properties and dielectric strength. In recent years, however, research efforts have been made to replace LN_2 with gaseous cryogens to take advantage of the broader temperature range of operation and the reduced risk of asphyxiation.[1–4] The wide temperature range provided by gaseous cryogens enables HTS cables and machines to carry higher current density and facilitates the integration of multiple cryogenic power devices into fewer cooling loops, which is systematically more efficient. As a part of this effort, the development of cryogenic power electronics,[5–7] cryogenic switchgear,[8] and HTS cables[9] has been researched. However, gaseous cryogens introduce two major shortcomings—(i) low heat capacity and (ii) low dielectric strength. Studies have shown that the low heat capacity can be partially resolved by increasing the pressure of the gas-cooled cryogenic system.[10] Moreover, the means of improving the dielectric strength of gaseous cryogenic media have been reported.[1–4,11–13] In these studies, the authors reported that the addition of small mole fractions of molecular gas species can substantially improve the dielectric strength of the gaseous cryogenic media.

As a continuation of the research on the development of superior dielectric media, here, we introduce a model that predicts the dielectric characteristics of supercritical He and Xe. Supercritical fluids are media achieved beyond the critical point. Conventionally, supercritical fluids have been widely used in chemical processes. Owing to the low polarizability and more easily achievable critical point (T_{cric} = 289.7 K and P_{cric} = 5.8 MPa), supercritical Xe proved itself to be a more beneficial solvent than SF_6 (T_{cric} = 318.51 K and P_{cric} = 3.749 MPa) and CO_2 (T_{cric} = 304.13 K and P_{cric} = 7.377 MPa)[14] and has been used in chemical reaction processes

and extractions of mixtures. For example, diamondoids, variants of the carbon cage molecule, and their derivatives were proposed as the future for nanotechnological devices and optoelectronic applications.[15] In synthesizing diamondoids, dielectric barrier discharge and pulsed laser ablation are generated in supercritical Xe as a precursor.[15] The same research group proposed to integrate the advantages of microreactors and microplasmas generated in supercritical Xe to synthesize diamondoids.[16] Moreover, the supercritical CO_2 Brayton power cycle has been used historically in optimizing the performance of line focusing solar power plants and reducing the cost of renewable energy.[17,18] In this context, the authors of Refs. 19 and 20 studied the alternatives of supercritical CO_2 and concluded that supercritical Xe is an important working fluid for future. The inert nature of Xe supports the low corrosion behavior, which is a key factor in saving the cost of power plant equipment. In a plasma thruster, supercritical Xe is stored in a propellent system to feed the thruster with appropriate mass flow rate and pressure because of its compatibility to high pressure and inert nature.[21–24]

More recently, supercritical fluids have been adopted as dielectric and thermal media as they show both liquid and gas properties simultaneously. The low viscosity comparable to that of gas provides effective heat transfer, while the high density comparable to that of liquid provides high dielectric strength, both of which lack in gaseous media.[25,26] For this reason, there is growing interest in researchers to use supercritical fluids in power applications.[27–31] For the applications of supercritical He and Xe in superconducting or cryogenic power systems and solar power plants, respectively, accurate dielectric strength modeling of supercritical He and Xe is integral. Accurate dielectric modeling of supercritical fluids is particularly important due to the steep decline of dielectric strength that occurs near the critical point. The drastic degradation in dielectric strength occurring near the critical point has been confirmed by experimental measurements.[25,32–36] The authors of these works have utilized the correlation between the density fluctuation caused by cluster formation near the critical point and breakdown voltage to explain the extreme degradation of dielectric strength. The reported correlation and models proposed in these studies mainly rely on the data of isothermal compressibility, which also vary near the critical point, retrieved from the NIST database.[37] However, difficulties may arise for modeling the dielectric strength of the fluids whose isothermal compressibility data are not available. To overcome the potential limitations, we model the dielectric strength variation of supercritical fluids by developing the electron scattering cross section data of clusters that form near the critical point.[29] In Ref. 38, the author formulated an expression to obtain electron scattering cross section data for any cluster size with respect to electron energy. This expression of the electron scattering cross section for a cluster includes the electron scattering cross section data of the gaseous molecule and probability of electrons to escape out from the cluster when the collision occurs due to ionization. The former account for the energy loss rate inside the cluster. The authors applied their formulated electron scattering cross section expression to H_2, N_2, and CO_2 and found satisfactory agreement between experimentally and numerically obtained values. In our work, we applied the approach to develop the electron scattering cross section data of He and Xe of various cluster sizes utilizing the electron scattering cross section data of their gaseous phase. The developed cross section data are subsequently incorporated into the electron kinetic analysis process (i.e., Boltzmann analysis) that yields the density-reduced critical electric field, which has been widely used for representing the dielectric strength of gases.[39–45] Instead of relying on the isothermal compressibility data, we develop a correlation between the dielectric strength and cluster size of supercritical He and Xe near the critical point. The dielectric strength is estimated based on the electron scattering cross section data of He and Xe clusters of various sizes. Because the electron scattering cross section data of He and Xe clusters are not available in the literature, we model them from the cross section data of gaseous He[46] and Xe.[47] Then, the dielectric strength of supercritical He and Xe is obtained by solving the Boltzmann equation, which is a widely used method of obtaining electron swarm parameters such as the density reduced ionization coefficient (α/N') and attachment coefficient (η/N') that describe the rate of free electron production and absorption. Based on the electron scattering cross section data of He and Xe derived for various cluster sizes, the Boltzmann equations are solved with the two-term approximation method.[48] A constant rate of attachment process is assumed for all cluster sizes as He and Xe inherently do not have electron attachment cross sections. The density reduced ionization coefficient exceeds the attachment process beyond the density reduced critical electric field $[(E/N')_{cr}]$ that represents the dielectric strength of supercritical He and Xe of various cluster sizes. The results of the proposed modeling approach are compared with experimental data reported in the literature to confirm the validity of the proposed modeling approach for He and Xe.

II. ELECTRON SCATTERING CROSS SECTION DATA OF CLUSTERS

For the simplicity of our electron scattering cross section data modeling approach, we assume a sphere with radius R_c as the cluster of both He and Xe near the critical point, as shown in Fig. 1. At point A, the electron enters the cluster and traverses following the horizontal trajectory. Collisions occur between points B and B' distanced by dx as the electron travels along the trajectory. The electron scattering cross section is multiplied by the cluster impact parameter, h, which is the normal distance between the center of the cluster and the electron trajectory. The total electron scattering cross section, σ, for cluster size N is derived by applying the following equation:[29,38,49]

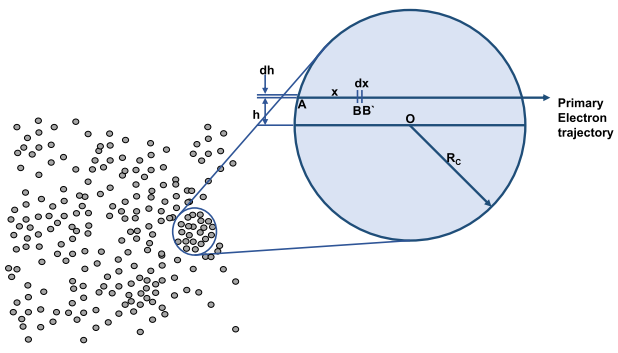

FIG. 1. Spherical electron–cluster collision model.

$$\sigma(N, W_{e0}) = \frac{\left[2\pi \int_0^{R_c} h\left\{1 - \exp\left[-n_0 \int_0^{2\sqrt{(R_c^2 - h^2)}} \sigma_0(1, W_e(x))F(x)dx\right]\right\}dh\right]}{N}, \quad (1)$$

where W_{e0} is the initial electron energy upon impact, $\sigma(N, W_{e0})$ is the electron scattering cross section data of the cluster, n_0 is the molecular density of the cluster, $\sigma_0(1, W_e(x))$ is the electron scattering cross section data of gaseous He and Xe, and $F(x)$ is the probability of secondary electrons being produced by ionization collisions escaping out of the cluster. It should be noted that $F(x)$ is only relevant to the ionization collision process. For this reason, for cross sections except for the ionization cross section, e.g., momentum transfer and excitation, $F(x)$ is not applicable. In our study, we define $F(x)$ with a three-dimensional spherical model, as shown in Fig. 2. We have assumed that clusters are spherical in shape. To model the probability of electrons escaping out of the cluster after an ionization collision, we assumed a sphere at the position of the electron on the trajectory inside the cluster. The escaping probability of an electron asymptotes to unity as the ionization occurs closer to the surface of the cluster. In this work, the probability of escaping out of the cluster due to ionization is formulated as the ratio of the spherical volume traveled by the electron to the total volume of the spherical cluster. The following equation represents the probability function:[29]

$$F(x) = (V_{cluster} - V_{sphere})/V_{cluster}, \quad (2)$$

where $V_{cluster}$ is the volume of the spherical cluster and V_{sphere} is the volume of a sphere that evolves with radii $(x_{max} - x)/2$ with the traversing electron, as shown in Fig. 2, and is defined as

$$V_{sphere} = \frac{4}{3}\pi\left(\frac{x_{max} - x}{2}\right)^3, \quad (3)$$

where x is the distance traveled by the electron inside the cluster along the trajectory and x_{max} is the maximum length an electron can travel with a cluster impact parameter h defined as the following equation:

$$x_{max} = 2\sqrt{(R_c^2 - h^2)}, \quad (4)$$

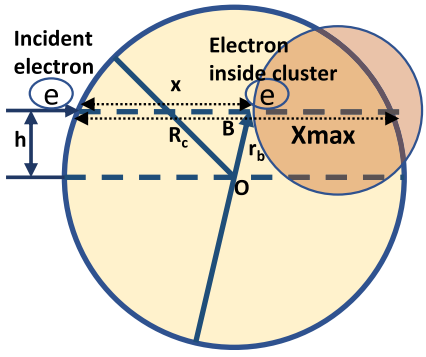

FIG. 2. Spherical model used for escape probability function $F(x)$.

where R_c is the radius of the cluster. The radius of the cluster shows a correlation with the cluster size N by the following equation:[38]

$$R_c = \sqrt[3]{\frac{3NM}{4\pi\rho}}, \quad (5)$$

where M is the mass of the gas molecule and ρ is the specific mass of the cluster. Figure 3 shows the probability function $F(x)$ as a function of the position of the electron along the trajectory of supercritical He. As shown by Fig. 3, the probability increases as the ionization collision takes place closer to the vicinity of the cluster surface.

The electron scattering cross section data of clusters in our model include the electron energy $W_e(x)$ at position x inside the cluster. The electron energy gradually decreases from its initial energy W_{e0} while traversing along the trajectory inside the cluster. At any position x on the trajectory, $W_e(x)$ is modeled as

$$W_e(x) = W_{e0} - \int_0^x \left(\frac{dW_e}{ds}\right)ds, \quad (6)$$

where W_{e0} is the electron energy at the moment of impact with the cluster and dW_e/ds is the energy loss rate of an electron traversing in the cluster. The energy loss rate of an electron inside the cluster shows different behaviors for different energy levels. For an electron energy level higher than 80 eV, the behavior of the energy loss rate is modeled by Bethe's formula. However, when the electron energy level falls below the mean excitation energy, Bethe's formula does not agree well with the experiment. That is, at a low electron energy level, Bethe's formula calculates the lower electron energy loss rate

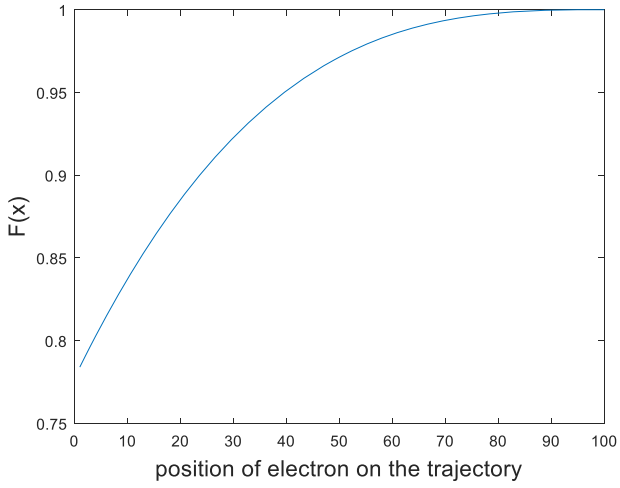

FIG. 3. Escaping out probability function F(x) of supercritical He.

than actual values, which cannot be explained. For this reason, for an energy level lower than 80 eV, all the energy loss mechanisms, such as ionization, excitation, and momentum transfer processes, are taken into account in modeling the electron energy loss rate. The electron energy loss rate we develop in our study is described as follows:

$$\frac{dW_e}{ds} \cong \begin{cases} -\frac{\alpha_1 z}{W_e}\ln\left(\frac{\alpha_2 W_e}{z}\right)\text{eV m}^{-1}, & W_e \geq 80\ \text{eV} \quad (7a) \\ -n\sigma_\tau\left((V_i + W_{s0})\alpha_i + \sum_{m,n} V^*_{m,n}a_{m,n} + 2\frac{m_e}{M}W_e\alpha_d\right)\text{eV m}^{-1}, & W_e \leq 80\ \text{eV}, \quad (7b) \end{cases}$$

where in the first equation $\alpha_1 = k_1 q^2 n/(8\pi\varepsilon_0)$, W_e is the electron energy, n is the density of the cluster, k_1 is the empirical factor of correction, z is the atomic number, and q is the elementary charge. For both He and Xe, we use 0.5 for k_1. In the second equation, σ_τ is the total collision cross section, $\alpha_i\sigma_\tau$ is the ionization cross section, W_{s0} is the mean initial energy of an electron ejected by an ionization collision, $\alpha_{m,n}\sigma_\tau$ is the excitation cross section, $\alpha_d\sigma_\tau$ is the momentum transfer cross section, V_i is the ionization potential, $V_{m,n}$ is the excitation potential, m_e is the mass of an electron, and M is the mass of a neutral. To show the effect of electron energy level on the rate of electron energy loss, the reduction of the electron energy inside the He cluster is represented in Fig. 4. It is observed from Fig. 4 that the electron loses energy as it travels along the trajectory. It decreases rapidly when the energy level is high, and after a certain distance when the energy falls below 80 eV, the energy loss rate reduces. For Xe, the electron energy inside the cluster shows a similar trend—if the energy is higher than 80 eV, the loss rate follows Bethe's formula, and when it falls below 80 eV, all energy loss mechanisms are used to calculate the energy loss rate. However, the loss rate of electron inside the Xe cluster is different from that of the He cluster because of the dependence of the loss rate on their physical properties, as shown in Eq. (7). The number density n_0 of a cluster is higher than that of gas. Since the ideal gas law becomes less applicable as it gets closer to the critical point, we modified the equation of state to account for the particle number density near the critical point. For this purpose, in our cross section data modeling, we introduce a density correction factor ρ_f. The ideal gas density is multiplied by the density correction factor, and the cross section data of a cluster containing a single particle are obtained. When the ideal gas density is multiplied by ρ_f, ionization coefficient values obtained from the cross section data of the one-particle cluster should agree with those obtained from the cross section data of the gas. For this reason, in our model, the value of ρ_f is different for different species. The following equation is used to define the number density:

$$n_0 = \frac{\rho_f P_c}{kT_c}, \quad (8)$$

where T_c is the critical temperature, P_c is the critical pressure, k is the Boltzmann constant, and ρ_f is the density correction factor. The ionization coefficient for a cluster containing one particle (i.e., cluster size 1) should be identical to that of the gaseous molecule of the same species. For this reason, a density correction factor ρ_f is determined for each species such that when the ideal gas density of the cluster with one particle is multiplied by ρ_f, it results in the same ionization coefficient as that of the gaseous molecule. Based on our modeling, ρ_f is 2 for He and 6 for Xe.

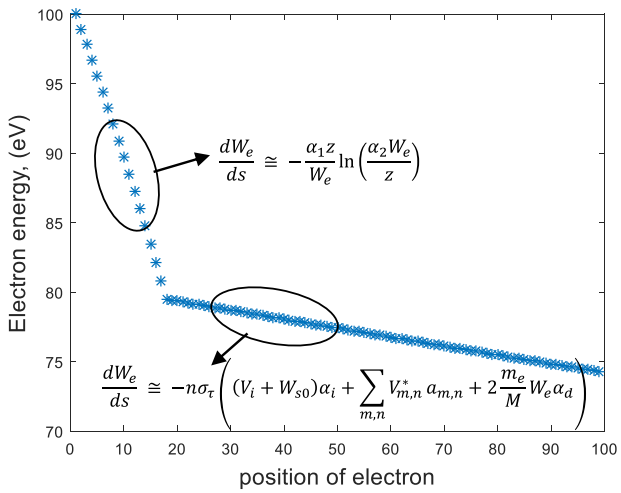

FIG. 4. Electron energy loss inside a cluster. Note that this is a generalized curve that applies to both He and Xe.

III. DENSITY REDUCED CRITICAL ELECTRIC FIELD

The Boltzmann analysis performed based on the electron scattering cross section data is a widely used method for obtaining the ionization coefficient and attachment coefficient.[1–4] For any occurrence of collisions by electrons in the molecule, the Boltzmann analysis determines the rate coefficients and the transport coefficients by solving the following Boltzmann equation:[48]

$$\frac{\partial f}{\partial t} + \vartheta \cdot \Delta f - \frac{e}{m}E \cdot \nabla_\vartheta f = C[f], \quad (9)$$

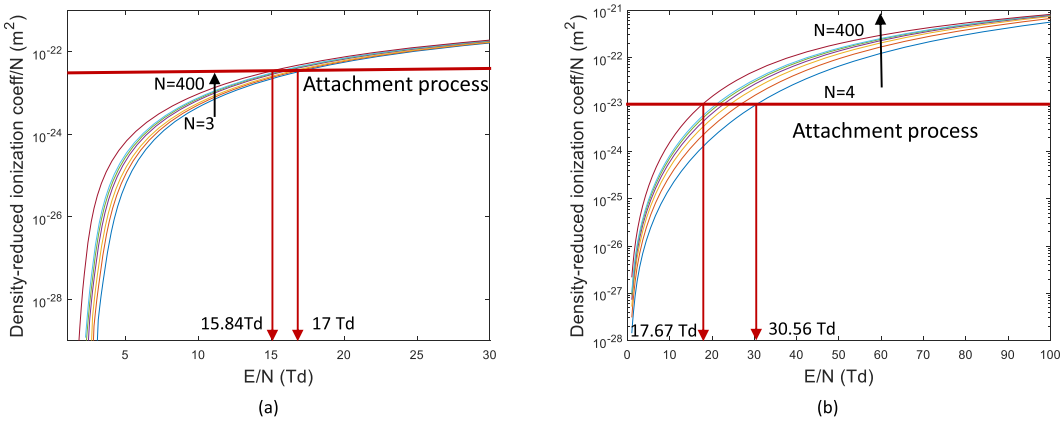

FIG. 5. Density reduced ionization coefficient for various cluster sizes, (a) supercritical He and (b) supercritical Xe.

where f is the electron distribution function in the phase space, ϑ is the velocity vector, e is the elementary charge, m is the mass of an electron, E is the electric field, ∇_v is the velocity gradient, and $C[f]$ is the rate of change in f due to collision. In this study, we numerically solve the Boltzmann equation with two-term approximation based on our modeled electron scattering cross section data of supercritical He and Xe of various cluster sizes near the critical point with the BOLSIG + solver. It has been reported that the two-term approximation method is less reliable at high E/N', in which the inelastic collision process is dominant, and the electron distribution is highly anisotropic. The Boltzmann analysis of the present study involves gas species that have large elastic momentum-transfer electron scattering cross sections and $(E/N')_{cr}$ as high as 46 Td for Xe and 17 Td for He.[48] The analysis results describe the kinetic processes of electrons that are represented by the density reduced ionization coefficient α/N' and density reduced attachment coefficient η/N'. The critical electric field at which the ionization process is in equilibrium with the electron attachment process has been used as the metric of comparing the dielectric strength of various gas media in numerous studies. The values of α/N' of supercritical He clusters and supercritical Xe clusters are plotted as a function of density reduced electric field E/N' to describe the kinetic process of electrons, as shown in Fig. 5. The point, where the ionization coefficient is in equilibrium with the attachment process, defines the density reduced critical electric field $(E/N')_{cr}$ that is used for estimating the dielectric strength of supercritical He and supercritical Xe near the critical point. He and Xe are non-electronegative gases. Hence, attachment cross section data are not available for He and Xe. Thus, a constant attachment process is assumed for both supercritical He and Xe—the value used for He is 3.5×10^{-23} m^2 and the value used for Xe is 1×10^{-23} m^2, as shown in Fig. 5. In this study, our objective is to model the dielectric strength variation of supercritical fluids, which shows good agreement with the experimental data. α/N' for each cluster size are already obtained based on the electron scattering cross section data. Therefore, η/N' is modeled such that the resulting dielectric strength variation shows close agreement with the experimental data. Figure 5(a) shows that $(E/N')_{cr}$ decreases from 17 Td to 15.84 Td with increasing cluster sizes of supercritical He when η/N' is modeled as 3.5×10^{-23} m^2. Similarly, in Fig. 5(b), $(E/N')_{cr}$ decreases from 30.56 Td to 17.67 Td when the cluster size of supercritical Xe increases, while η/N' is kept at 1×10^{-23} m^2.

IV. RESULTS AND DISCUSSION

A. Modeled results of cluster cross section data

The electron scattering cross section data of gaseous He retrieved from the Phelps database[46] and gaseous Xe retrieved from the SIGLO database[47] are applied to Eq. (1) to derive the electron scattering cross section data of supercritical He and supercritical Xe near its critical point—T_{cric} = 5.25 K and p_{cric} = 0.227 MPa for He, and T_{cric} = 289.733 K and p_{cric} = 5.842 MPa for Xe. As an example, we show the momentum transfer, excitation, and ionization cross section data of supercritical He with cluster size N = {11, 52, 91} and the corresponding cross section data of gaseous He in Fig. 6(a) and the elastic, excitation, and ionization cross section data of supercritical Xe with cluster size N = {11, 50, 100} and the corresponding cross section data of gaseous Xe in Fig. 6(b). A reduction in the cross sections is observed with the increasing cluster size from that of gaseous He and gaseous Xe. The phenomenon of cross section reduction agrees well with results previously reported in the literature by experiments conducted on clustered molecules.[50,51] In addition to this, the authors in their previous studies[25,32,33,35,36] confirmed the decrease in the cross sections with increasing cluster size by forming a correlation between the breakdown voltage near the critical point and density fluctuation. In Fig. 6(a), momentum transfer, excitation, and ionization cross sections show significant changes at an electron energy level below 100 eV. However, at electron energy above 100 eV, the changes in cross section values are not as drastic as those in lower electron energy. In this model, we utilize the cross section data of gaseous He and Xe to derive the cross section data of He and Xe clusters. The electron energy corresponds to each cross section value of gaseous He[46] and Xe.[47] In this study, we determine the electron energy at each position in the cluster by utilizing Eq. (6) and define the cross section value closest to each electron energy in the PHELPS database[46] as $\sigma_0(1, W_e(x))$. Consequently, at a high electron energy level, the cross sections maintain constant values over certain

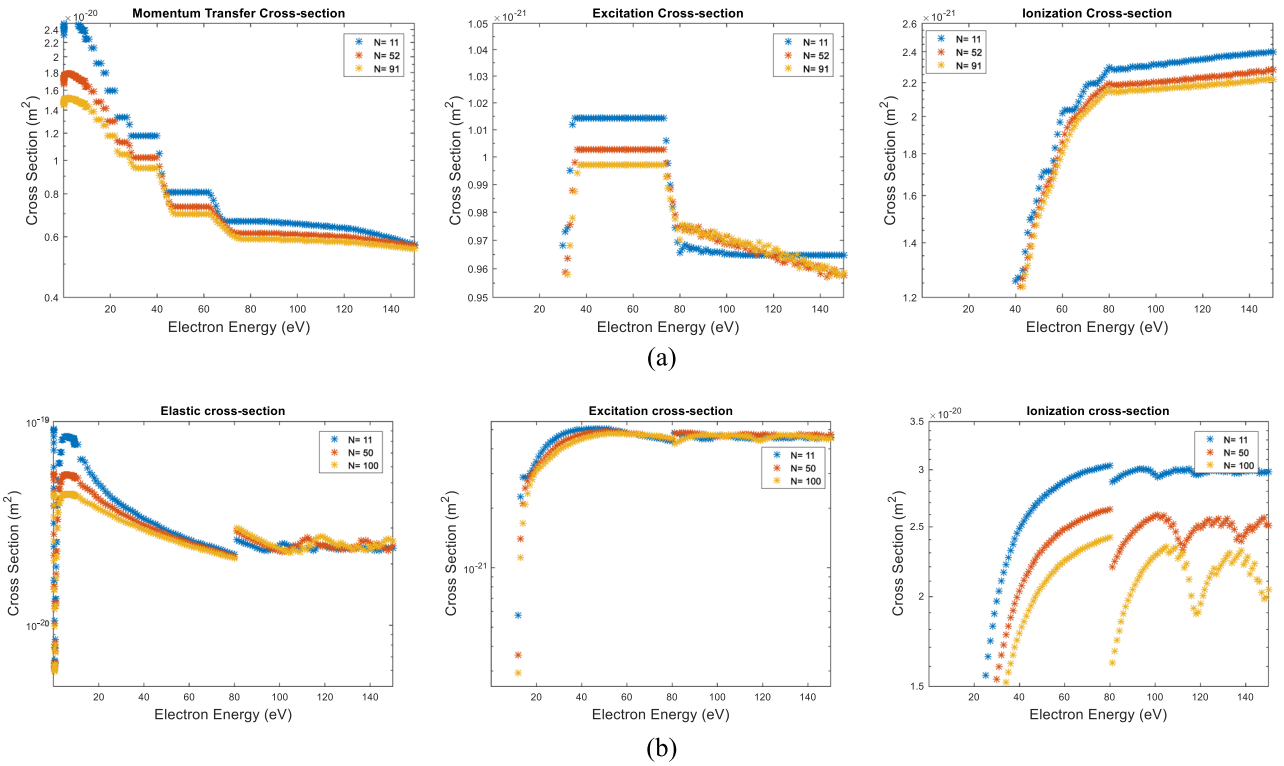

FIG. 6. (a) Momentum transfer, excitation, and ionization cross section data of the He cluster with respect to initial electron impact energy and (b) elastic, excitation, and ionization cross section data of the Xe cluster with respect to initial electron impact energy.

electron energy ranges and reduce at the subsequent electron energy ranges. For this reason, the staircase characteristics of the cross section data are shown in Fig. 6(a). The derived electron scattering cross sections of He and Xe clusters are used in the Boltzmann analysis to obtain α/N' and η/N'.

B. Modeled results of the dielectric strength variation

The dielectric strength of supercritical He and supercritical Xe is estimated by the critical electric field E_{cr}, derived from various cluster sizes near the critical point. Figure 7 shows E_{cr} as a function of pressure for supercritical He and Xe. In Fig. 7(a), E_{cr} of supercritical He is plotted over a constant temperature of 5.25 K. It is observed from Fig. 7(a) that near the critical pressure, a steep decline in the breakdown electric field occurs. Compared to the experimental data in the literature,[35] the modeled data of this study show close agreement in dielectric strength near the critical pressure. Similarly, experimental data of breakdown electrical fields at temperatures 5.10 K and 5.40 K, reported in Ref. 35, are plotted as a function of pressure in Fig. 7(a). It is observed that at temperature below and above the critical point, a comparatively less steep decline in dielectric strength is observed. In Fig. 7(b), E_{cr} of supercritical Xe for a constant temperature of 289.73 K is plotted and a steep decline of the breakdown electric field is observed near the critical pressure. The modeled data based on the cross section data of clusters are compared with the experimental values measured at a temperature of 292.15 K.[34] It is observed that our approach of modeling the dielectric variation of supercritical Xe near the critical point results in very close agreement with the experimental data. Since experimental data on the cluster size of supercritical fluids are not reported in the literature, we assumed the cluster sizes near the critical point, as shown in Fig. 7. The goal of this work is to model the substantial degradation of the dielectric breakdown electric field that takes place near the critical point in effect of the molecular clustering. Moreover, our model signifies its validity when compared with the experimental data with some discrepancies. If the cluster size of supercritical fluids near the critical point can be measured, the discrepancies can be reduced. If we correlate our modeled data and the assumed cluster sizes, it is observed that for supercritical He, the dielectric variation model matches with the experimental values when the largest cluster size is 400 with 15% discrepancies between modeled data and experimental data when η/N' is 3.5×10^{-23} m^2 at a critical point. Again, for supercritical Xe at a critical point, discrepancies between the modeled data and experimental data are 22% with the largest cluster size assumed to be 400 for η/N' being 1×10^{-23} m^2.

C. Discussion

Supercritical fluids show inhomogeneity in microscale, while in macroscale, the structure of the fluid appears to be homogeneous.[25]

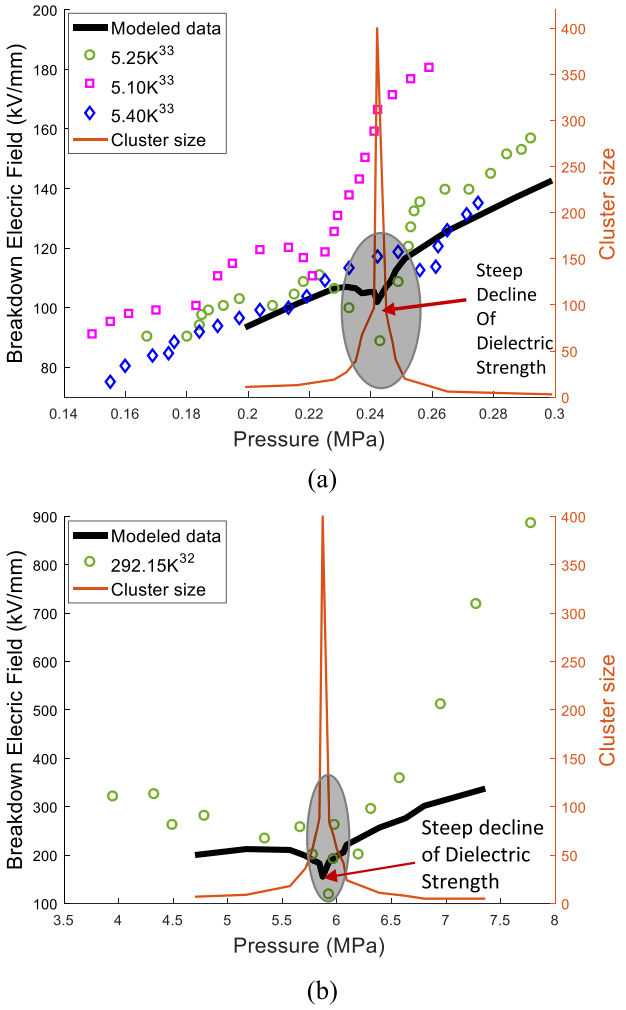

FIG. 7. Dielectric strength of (a) supercritical He and (b) supercritical Xe.

For micrometer-scale discharge generated with very small electrodes' gap distance, the surface/volume ratio is high enough to allow clearing out the heat generated in the discharge space. This, in effect, supports to maintain the clusters' structure. However, when there is a substantial gap distance, the temperature of the space caused by the discharge becomes locally higher than the critical temperature, which in effect destroys the molecular clustering.[34] Although dielectric properties and discharge characteristics vary depending on the gap distance, our approach only applies to local electron kinetics and thus does not account for gap-length-induced phenomena in the estimation of dielectric strength.

V. CONCLUSIONS

In this work, we utilized a modeling approach that is based on the cross section data of clusters to estimate the dielectric strength of supercritical He and Xe near the critical point. We modeled the electron scattering cross sections of supercritical He and supercritical Xe of various cluster sizes near the critical point based on which the Boltzmann analysis was performed to obtain the breakdown electric field. Sharp declines in the breakdown electric field were observed near the critical point, which suggest the increase of mean free path due to the formation of clusters and density fluctuations. The agreements achieved between the modeled data using the electron scattering cross sections of He and Xe clusters near the critical point and the experimental breakdown measurements near the critical point confirm the validity of our modeling approach.

DATA AVAILABILITY

The data that support the findings of this study are available within the article.

REFERENCES

[1]C. Park, S. Pamidi, and L. Graber, "Boltzmann analysis of cryogenic He–H_2 gas mixtures as dielectric media for high-temperature superconducting power devices," IEEE Trans. Appl. Supercond. **27**, 1 (2017).
[2]C. Park, S. Pamidi, and L. Graber, "The critical electric field of gas mixtures over the extended range of cryogenic operating conditions," J. Appl. Phys. **122**, 153301 (2017).
[3]C. Park, L. Graber, and S. Pamidi, "The dielectric properties of gaseous cryogen mixtures of He, H_2, Ne, and N_2 in a temperature range of 50–80 K at pressures up to 2.0 MPa," J. Appl. Phys. **121**, 083304 (2017).
[4]C. Park, S. Pamidi, and L. Graber, "The dielectric strength of dissociated cryogenic gas media," J. Appl. Phys. **124**, 104104 (2018).
[5]L. Graber, M. Saeedifard, M. J. Mauger, Q. Yang, C. Park, T. Niebur, S. V. Pamidi, and S. Steinhoff, "Cryogenic power electronics at megawatt-scale using a new type of press-pack IGBT," IOP Conf. Ser.: Mater. Sci. Eng. **279**, 012011 (2017).
[6]C. Park, M. J. Mauger, T. Damle, J. Huh, S. Steinhoff, and L. Graber, "Cryogenic power electronics: Press-pack IGBT modules," IOP Conf. Ser.: Mater. Sci. Eng. **756**, 012009 (2020).
[7]C. Park, O. Obadolagbonyi, and L. Graber, "Cryogenic power electronics: Capacitors and inductors," IOP Conf. Ser.: Mater. Sci. Eng. **756**, 012010 (2020).
[8]C. Xu, R. Saluja, T. Damle, and L. Graber, "Future cryogenic switchgear technologies for superconducting power systems," IOP Conf. Ser.: Mater. Sci. Eng. **279**, 012012 (2017).
[9]P. Cheetham, H. Ravindra, T. Stamm, C. Park, C. Kim, L. Graber, M. Steurer, and S. Pamidi, in *2019 IEEE Electric Ship Technology Symposium (ESTS)* (IEEE, Washington, DC, USA, 2019), pp. 548–555.
[10]S. Pamidi, C. H. Kim, J.-H. Kim, D. Crook, and S. Dale, "Cryogenic helium gas circulation system for advanced characterization of superconducting cables and other devices," Cryogenics **52**, 315 (2012).
[11]C. Park, L. Graber, P. Cheetham, J. G. Viquez, C. H. Kim, and S. Pamidi, "A versatile modeling technique for predicting dielectric strength improvements in gas mixtures for superconducting applications," IEEE Trans. Dielectr. Electr. Insul. **24**, 2755 (2017).
[12]C. Park, S. Pamidi, and L. Graber, "Evaluating the dielectric strength of helium-nitrogen gas mixtures by plasma parameter measurements," Phys. Plasmas **25**, 043520 (2018).
[13]C. Park, L. Graber, P. Cheetham, A. Al-Taie, S. Telikapalli, and S. Pamidi, "Versatile Paschen's model for the dielectric strength estimation of binary and ternary gas mixtures," IEEE Trans. Dielectr. Electr. Insul. **26**, 1569 (2019).
[14]R. D. Smith, S. L. Frye, C. R. Yonker, and R. W. Gale, "Solvent properties of supercritical xenon and sulfur hexafluoride," J. Phys. Chem. **91**, 3059 (1987).
[15]T. Shizuno, H. Miyazoe, K. Saito, S. Stauss, M. Suzuki, T. Sasaki, and K. Terashima, "Synthesis of diamondoids by supercritical xenon discharge plasma," Jpn. J. Appl. Phys. **50**, 030207 (2011).
[16]F. Oshima, S. Stauss, C. Ishii, D. Z. Pai, and K. Terashima, "Plasma microreactor in supercritical xenon and its application to diamondoid synthesis," J. Phys. Appl. Phys. **45**, 402003 (2012).

[17]K. Ravi Kumar and K. S. Reddy, "4-E (energy-exergy-environmental-economic) analyses of line-focusing stand-alone concentrating solar power plants," Int. J. Low Carbon Technol. **7**, 82 (2012).
[18]N. B. Desai and S. Bandyopadhyay, "Line-focusing concentrating solar collector-based power plants: A review," Clean Technol. Environ. Policy **19**, 9 (2017).
[19]L. Coco-Enríquez, J. Muñoz-Antón, and J. M. Martínez-Val, "New text comparison between CO_2 and other supercritical working fluids (ethane, Xe, CH_4 and N_2) in line-focusing solar power plants coupled to supercritical Brayton power cycles," Int. J. Hydrogen Energy **42**, 17611 (2017).
[20]L. Coco-Enríquez, J. Muñoz-Antón, and J. M. M.-V. Peñalosa, "Comparison between s-CO_2 and other supercritical working Fluids (s-Ethane, s-SF_6, s-Xe, s-CH_4, s-N_2) in line-focusing solar power plants with supercritical Brayton power cycles," in Proceedings of the European Conference Renewable Energy ECRES, Istanbul, Turkey,, 7 (2016).
[21]Y. Fendler, S. Carpentier, P. Barbier, F. Martin, E. Guilbaud, and C. Boniface, in 35th International Electric Propulsion Conference, October, 2017.
[22]F. Trezzolani, M. Manente, E. Toson, A. Selmo, M. Magarotto, D. Moretto, and D. Pavarin, in 35th International Electric Propulsion Conference, IEPC-2017-519, Atlanta, Georgia, USA, October, 2017.
[23]T. A. Collard, J. P. Sheehan, and A. D. Gallimore, presented at Joint Conference of 30th International Symposium on Space Technology and Science, 34th International Electric Propulsion Conference and 6th Nano-Satellite Symposium, Hyogo-Kobe, Japan, July, 2015.
[24]D. Manzella, S. Oleson, J. Sankovic, T. Haag, A. Semenkin, and V. Kim, in *32nd Joint Propulsion Conference and Exhibit* (American Institute of Aeronautics and Astronautics, Lake Buena Vista, FL, USA, 1996).
[25]S. Stauss, H. Muneoka, K. Urabe, and K. Terashima, "Review of electric discharge microplasmas generated in highly fluctuating fluids: Characteristics and application to nanomaterials synthesis)," Phys. Plasmas **22**, 057103 (2015).
[26]J. Wei, A. Cruz, C. Xu, F. Haque, C. Park, and L. Graber, in *2020 IEEE Electrical Insulation Conference (EIC)* (IEEE, Knoxville, TN, USA, 2020), pp. 107–113.
[27]C. Xu, J. Wei, and L. Graber, in *2020 IEEE Electrical Insulation Conference (EIC)* (IEEE, Knoxville, TN, USA, 2020), pp. 171–174.
[28]Y. Tian, J. Wei, C. Park, Z. Wang, and L. Graber, in *2018 12th International Conference on the Properties and Applications of Dielectric Materials (ICPADM)* (IEEE, Xi'an, 2018), pp. 992–995.
[29]F. Haque, J. Wei, L. Graber, and C. Park, "Modeling the dielectric strength variation of supercritical fluids driven by cluster formation near critical point," Phys. Fluids **32**, 077101 (2020).
[30]J. Wei, C. Park, and L. Graber, "Breakdown characteristics of carbon dioxide-ethane azeotropic mixtures near the critical point," Phys. Fluids **32**, 053305 (2020).
[31]J. Wei, A. Cruz, F. Haque, C. Park, and L. Graber, "Investigation of the dielectric strength of supercritical carbon dioxide-trifluoroiodomethane fluid mixtures," Phys. Fluids **32**, 103309 (2020).
[32]T. Ito and K. Terashima, "Generation of micrometer-scale discharge in a supercritical fluid environment," Appl. Phys. Lett. **80**, 2854 (2002).
[33]T. Ito, H. Fujiwara, and K. Terashima, "Decrease of breakdown voltages for micrometer-scale gap electrodes for carbon dioxide near the critical point: Temperature and pressure dependences," J. Appl. Phys. **94**, 5411 (2003).
[34]M. Sawada, T. Tomai, T. Ito, H. Fujiwara, and K. Terashima, "Micrometer-scale discharge in high-pressure H_2O and Xe environments including supercritical fluid," J. Appl. Phys. **100**, 123304 (2006).
[35]H. Muneoka, K. Urabe, S. Stauss, and K. Terashima, "Breakdown characteristics of electrical discharges in high-density helium near the critical point," Appl. Phys. Express **6**, 086201 (2013).
[36]H. Muneoka, K. Urabe, S. Stauss, and K. Terashima, "Micrometer-scale electrical breakdown in high-density fluids with large density fluctuations: Numerical model and experimental assessment," Phys. Rev. E **91**, 042316 (2015).
[37]E. Lemmon, M. McLinden, and D. Friend, *NIST Standard Reference Database 23: Reference Fluid Thermodynamic and Transport Properties—REFPROP, Version 9.0* (National Institute of Standards and Technology, Standard Reference Data Program, Gaithersburg, 2012).
[38]F. Bottiglioni, J. Coutant, and M. Fois, "Ionization cross sections for H_2, N_2, and CO_2 clusters by electron impact," Phys. Rev. A **6**, 1830 (1972).
[39]L. Zhong, A. Yang, X. Wang, D. Liu, Y. Wu, and M. Rong, "Dielectric breakdown properties of hot SF_6-2 mixtures at temperatures of 300–3500 K and pressures of 0.01–1.0 MPa," Phys. Plasmas **21**, 053506 (2014).
[40]W. Wang, X. Tu, D. Mei, and M. Rong, "Dielectric breakdown properties of hot SF_6/He mixtures predicted from basic data," Phys. Plasmas **20**, 113503 (2013).
[41]X. Wang, L. Zhong, M. Rong, A. Yang, D. Liu, Y. Wu, and S. Miao, "Dielectric breakdown properties of hot SF_6 gas contaminated by copper at temperatures of 300–3500 K," J. Phys. Appl. Phys. **48**, 155205 (2015).
[42]Y. Wu, W. Wang, M. Rong, L. Zhong, J. Spencer, and J. Yan, "Prediction of critical dielectric strength of hot CF_4 gas in the temperature range of 300-3500 K," IEEE Trans. Dielectr. Electr. Insul. **21**, 129 (2014).
[43]X. Li, H. Zhao, S. Jia, and A. B. Murphy, "Study of the dielectric breakdown properties of hot SF_6-CF_4 mixtures at 0.01–1.6 MPa," J. Appl. Phys. **114**, 053302 (2013).
[44]M. Yousfi, P. Robin-Jouan, and Z. Kanzari, "Electron-molecule collision cross sections needed for breakdown electric field calculations of hot dissociated SF_6," J. Phys.: Conf. Ser. **115**, 012012 (2008).
[45]A. V. Larin, N. Meurice, D. N. Trubnikov, and D. P. Vercauteren, "Theoretical analysis of the synergism in the dielectric strength for SF_6/CF_4 mixtures," J. Appl. Phys. **96**, 109 (2004).
[46]See http://www.lxcat.laplace.univ-tlse.fr for PHELPS database, retrieved on June 2013.
[47]See http://www.lxcat.laplace.univ-tlse.fr for SIGLO database, retrieved on June 2013.
[48]G. J. M. Hagelaar and L. C. Pitchford, "Solving the Boltzmann equation to obtain electron transport coefficients and rate coefficients for fluid models," Plasma Sources Sci. Technol. **14**, 722 (2005).
[49]F. Haque, J. Wei, L. Graber, and C. Park, in *2020 IEEE Electrical Insulation Conference (EIC)* (IEEE, Knoxville, TN, USA, 2020), pp. 144–147.
[50]A. N. Zavilopulo, A. I. Dolgin, and M. A. Khodorkovsky, "Investigation of argon cluster ionization cross sections by electron impact," Phys. Scr. **50**, 696 (1994).
[51]W. Henkes and F. Mikosch, "The effective cross section for ionization by electrons of molecules in hydrogen clusters," Int. J. Mass Spectrom. Ion Phys. **13**, 151 (1974).